ENERGY DISSIPATION MECHANISMS IN CERAMIC MATRIX COMPOSITES
Konstantinos G. Dassios

Energy dissipation in ceramic matrix composite (CMC) materials is controlled by two main mechanisms: fiber bridging and interfacial damage. The magnitude and interaction of these mechanisms are herein explained, mathematically formulated and phenomenologically convoluted in an expression that can directly assess the experimentally observed macromechanical response of CMCs. The expression is derived on the force-displacement domain and can be scaled up to predict the bridging stress versus crack opening displacement behaviour of the material. The theoretical predictions are compared to macromechanical experimental results from SiC-fibre reinforced glass matrix laminates of varying dimensions as well as real bridging stress values measured directly at the microscale using Laser Raman Miscoscopy on the same materials. The model was independently used to predict the mechanical response of hypothetical composite systems with different fibre and interfacial energy dissipation potentials. A dramatic dependence of interfacial shear stress on the mechanical performance was found and is discussed in the text.

INTRODUCTION

While ceramics combine unique thermal and mechanical properties, they suffer from extreme brittleness, hence also unstable catastrophic failure. These characteristics had limited their use in high temperature applications until the discovery of Ceramic Matrix Composites (CMCs) unleashed the potential of ceramics by introducing mechanisms that decreases the energy available for the catastrophic work of crack advance at the crack tip by consuming part of the externally applied energy. Significant improvements in crack growth resistance, damage tolerance, toughness and strength were achieved with the introduction of long, continuous fibres in CMCs, in the mid-1990s. Since then, the interest in ceramic matrix composite research has increased considerably and CMCs have efficiently replaced metals in applications such as aircraft brakes, thermal barriers, turbine nozzles, space shuttle parts and many more. The Space Shuttle Columbia disaster of February 1st, 2003, due to the failure of the Ceramic Matrix Composite panel on the leading edge of the Shuttle's left wing (NASA, 2003), draw new scientific interest in CMCs. Research is concentrated in understanding and quantifying the role of the energy dissipation mechanisms that develop during composite loading and determine the mechanical performance of the composite. Crack bridging by intact fibers and pull-out of failed fibers are the main energy dissipation mechanisms developing in CMCs, while interfacial debonding and crack deflection consume smaller amounts of energy. All four mechanisms are directly or indirectly related to the properties and performance of the interface, which, despite its small thickness, is essentially, responsible for the overall mechanical behaviour of the composite.

Conventional fracture mechanics approaches such as the R-curve (Cox, 1991; Fett, Munz and Geraghty, 2000) cannot approach the contributions and quantify the interactions of the composite phases *independently*, hence these approaches are incapable of assessing the contribution of the energy dissipation mechanisms in the mechanical response of the material. To overcome this shortcoming of fracture mechanics, various bridging laws have been proposed that correlate the stress on fibers bridging a macro-crack and the instant crack opening displacement (COD) (Foote, Mai and Cotterell, 1986). Currently available bridging laws are formulated based on theoretical approaches such as statistics (Sutcu, 1989; Thouless and Evans, 1988; Llorca and Singh, 1991), micromechanical models (Rausch, Kuntz and Gratwohl, 2000), J-integral considerations (Sorensen and Jacobsen, 1998; Jacobsen and Sorensen, 2001), compliance approaches (Hu and Mai, 1992; Pappas

and Kostopoulos, 2001), and stress intensity (Fett and Munz, 1995). The major problem in such previous studies is that, by considering the bridging mechanism alone, the contribution of the pull-out mechanism, which appears after the first fibre failure and grows to dominant extents, is overlooked. To this end, we have already shown that using simple Weibull statistics concepts and rational conditions, a fracture law can be developed that assesses the mechanical behaviour of the composite (Dassios, Kostopoulos and Steen, 2007). Another shortcoming of the bridging law approach is the lack of experimental values of bridging stress from CMCs that are needed to validate the theoretical predictions. To this end, Laser Raman Microscopy (LRM) is a leading technique in capturing real-time stress and strain values at the microscale. We have shown that the use of LRM can be extended to measuring bridging stresses on individual fibres in ceramic matrix composites, in situ during testing (Dassios et al, 2003b).

We present herein a phenomenological model for the assessment of the mechanical response of ceramic matrix composites and we validate it across real, in situ measurements of bridging stresses captured at the microscale on a CMC using LRM. The model is based on the addition of the contributions of the matrix, fibres and interface to the total mechanical response of the composite. The formulation is derived on the force-displacement domain to capture the originally recorded behaviour and is scaled up to predict the bridging stress of the material. Model usage is not exclusive to CMCs and can be extended to any brittle-matrix composite system exhibiting similar energy dissipation characteristics. The model is employed to understand the role of key material properties in the overall macromechanical response of the CMCs while the ability of the model to *predict* the fracture behaviour of such materials composite is discussed.

THEORETICAL

Energy dissipation in brittle-matrix composites
Stable crack growth in a ceramic matrix composite with a moderately strong interface (weak enough for debonding, strong enough for efficient stress transfer) under Mode I loading commences with an increase in the system's energy due to external loading. A crack propagates from a notch root or a critically-sized defect in the matrix when the fracture toughness value K_I, or energy G_I, associated with the notch or defect exceeds the critical values, K_{Ic}, or G_{Ic} respectively. With further energy input, the crack tip will extend and reach the fiber boundary where it will deflect along the fiber/matrix interface causing *interfacial debonding* (Fig. 1a). With further loading, the energy consumed in debonding will eventually balance the work required for further crack growth and the crack will propagate along the energetically most preferable path. The crack will have *deflected* if the new crack plane does not coincide with the plane of the initial notch. Behind the crack, intact fibers *bridging* the crack faces are stretching in air within that region while sliding of the fibers along the debonded interface gives rise to frictional forces (Fig. 1c). These fibers carry bridging stresses, thus they consume, locally, a portion of the external energy hence they decrease, by the same amount, the energy available for catastrophic crack growth. Debonding, deflection, bridging and sliding develop in a similar manner every time the advancing crack encounters new fibers (Fig. 1d). Further external energy input will eventually balance the critical energy for fiber fracture. This amount of energy is less than the value predicted by fiber strength because, in accordance with fracture mechanics expectations, real fibers are non-ideal media that contain flaws and fail at locations predetermined by their surface flaw distribution (Sutcu, 1989). It is then expected that fiber failure will not occur within the crack faces where fibers stretch freely but will confine within the debonded length where sliding of the fiber along the rough interface will render the dimensions of surface flaws to critical values. It has also been shown that

the debond length is usually much larger than the instant crack opening displacement, hence also by a mechanics of materials point of view, the probability of a fibre failing within the matrix environment (giving rise to pull-out) is much larger than the probability of failing within the crack faces (Dassios, 2003a). With further loading, fibers that have failed within the matrix environment will *pull-out* (Fig. 1c) while their sliding along the debonded interface will give rise to more frictional forces. The energy consumed as friction is the contribution of the interface to the total energy dissipation potential of the composite. This contribution can be significant depending on the interface and considering the vast surface area available for sliding around the fibers in a composite. After complete fibre failure, the pull-out mechanism is the sole mechanism controlling the composite's mechanical behaviour and remains active until all fibres tips have completely disengaged from the matrix environment.

Phenomenological model formulation
The model invokes the fundamental argumentation that the total load carried by the composite at each loading instance is the sum of loads carried by its constituents individually, namely the matrix, the fiber, and the interface. Based on the original Weibull distribution function rationale, we construct a two-parameter model that assesses the role of the matrix and fibres in the fracture procedure and a modified exponential decay function for the frictional pull-out contribution. The generalized forms of the proposed probability distribution function and cumulative distribution function, respectively, are given by:

$$f(x;a,b) = Cx\exp\left\{-(x/b)^a\right\} \quad x>0; a,b>0 \quad (1)$$

$$P(x;a,b) = 1 - \exp\left\{-(x/b)^a\right\} \quad (2)$$

where a is the shape parameter, b the scale parameter, and C is a constant. The appropriateness of Eq. 1 and 2 in describing the fracture of ceramic composite constituents, stems from the fact that they predict a linear response of the dependent variable for small x values, as encountered in a linear elastic regime, in combination with a steep decay at higher x values, compatible with a catastrophic, step-wise, fracture. Logical conditions are used to correlate the magnitudes and order of appearance of the individual contributions. The model assumes that equal strain conditions apply among the constituents, an assumption that is valid for extension-controlled loading.

To approach the matrix contribution to the total load of the composite we argue that crack propagation within matrix parts secluded between adjacent fibres or fibre bundles, as well as crack deflection, are mechanisms that contribute to a gradual matrix failure. The relevant distribution function that approaches the load carried by the matrix, $F_m(u)$ at a displacement u, follows from Eq. 0:

$$F_m(u) = C_m \cdot u \cdot e^{-\left(\frac{u}{b_m}\right)^{a_m}} \quad (3)$$

Fig. 1: Evolution of energy dissipation mechanisms during crack propagation in a brittle matrix a) First crack growth, crack front debonding and initial bridging, b) Extended bridging and sliding of intact fibers along the debonded interface, c) Fibre pull-out and fully developed mechanisms

slope of the curve, hence this term is the inverse elastic compliance of the matrix. Eq (3) then becomes:

$$F_m(u) = \frac{S(1-V_f)E_m}{l} \cdot u \cdot e^{-\left(\frac{u}{b_m}\right)^{a_m}} \tag{4}$$

Where l is the gauge length, S is the cross sectional area of the composite, V_f is the fibre volume fraction and E_m is the matrix elastic modulus.

The intact fibre contribution to total load-displacement response of the material can be written in analogy to Eq. 4 as:

$$F_f(u) = \frac{SV_fE_f}{l} \cdot u \cdot e^{-\left(\frac{u}{b_f}\right)^{a_f}} \tag{5}$$

where a_f and b_f are the shape and location parameters for the fibres and E_f is their elastic modulus.

The contribution of a moderate interface to the total load stems mainly from the shear forces that develop during sliding of intact and failed fibres along the debonded interface. Given the fact that deformation of intact fibres along the debonded interface (within the matrix environment) is very small compared to their deformation within the crack flanks, it is safe to assume that forces due to constrained sliding of intact fibres' surfaces along the debond length are negligible compared to forces developing during free sliding of pull-out fibres along the whole debond length. Then, a force balance around the fibre gives the axial component, f_i, of shear forces acting on a single fibre due to its interaction with the interface:

$$f_i = 2\pi R_f L_p \tau \tag{6}$$

where R_f is the fibre radius, L_p is the average pull-

In Eq. 3, a_m and b_m are the shape and location parameters of the distribution for the matrix. In the F-u domain, the term C_m should represent the initial

out length and τ is the shear strength of the interface. Eq. 6 holds for a single fibre. The total interfacial contribution to composite load, F_i, is the product of the right-scale of Eq. 6 and the total number of failed fibres pulling out of the matrix, N_{fail}, and can be expressed as:

$$F_i(u) = 2\pi R_f L_p \cdot \tau \cdot N_{fail}(u) \cdot \lambda(u) \tag{7}$$

where $\lambda(u)$ is the inactive fiber correction, accounting for decay in interfacial load due to successive disengaging of fiber tips from the matrix environment (complete pull-out). N_{fail} can be calculated from the total number of 0° fibres in the composite that are available for pull-out, N_{0°, and the proposed cumulative distribution function (eq 2), as:

$$\frac{N_{fail}(u)}{N_{0^\circ}} = 1 - e^{-\left(\frac{u}{b_f}\right)^{a_f}} \tag{8}$$

In turn, N_{0° can be calculated by the total volume occupied by 0° fibres in the composite as:

$$N_{0^\circ} \pi R_f^2 = SV_f k \tag{9}$$

where k is the fraction of fibres contributing to pull-out. In a symmetrically stacked laminate, k=0.5.
Based on a previous proof that the decrease in load due to pull-out of failed fibres follows a first order exponential decay function with a decay constant equal to the mean pull-out length, L_p, (Sutcu, 1989). the inactive fibre correction can be expressed as:

$$\lambda(u) = e^{-\frac{u}{L_p}} \tag{10}$$

Using Eq. 8, 9 and 10, the interfacial contribution to composite load, Eq. 7, can be written as:

$$F_i(u) = \frac{2SV_f kL_p \tau}{R_f} \left(1 - e^{-\left(\frac{u}{b_f}\right)^{a_f}} \right) e^{-\frac{u}{L_p}} \tag{11}$$

The interfacial contribution becomes active only after first fiber failure, hence Eq. 11 must be shifted in to the right by the instant displacement on the onset of fibre fracture, u^*:

$$F_i(u) = \frac{2SV_f kL_p \tau}{R_f} \left(1 - e^{-\left(\frac{u-u^*}{b_f}\right)^{a_f}} \right) e^{-\frac{u-u^*}{L_p}} \tag{12}$$

The total load-displacement behaviour of the composite can be expressed as the sum of the individual contributions, Eq. (4), (5) and (12):

$$F_{comp}(u) = \frac{SV_f}{l} \left\{ \begin{array}{l} \dfrac{1-V_f}{V_f} E_m u\, e^{-\left(\frac{u}{b_m}\right)^{a_m}} + E_f u\, e^{-\left(\frac{u}{b_f}\right)^{a_f}} + \\[2em] + \dfrac{2klL_p\tau}{R_f} \left[e^{-\frac{u-u^*}{L_p}} - e^{-\frac{u-u^*}{L_p} - \left(\frac{u-u^*}{b_f}\right)^{a_f}} \right] \end{array} \right\} \tag{13}$$

In brittle-matrix composite fracture, any non-linear contribution to the recorded load stems from irreversible damage such as the bridging and pull-out mechanisms. Likewise, in tensile specimen configurations, the displacement recorded in the non-linear regime corresponds purely to crack flank separation, i.e. crack opening displacement. Then, the bridging stress can be obtained by excluding the elastic displacement from the stress-equivalent of Eq. 13. In practice, the subtraction of the elastic displacement from the total displacement of the system, gives the crack opening displacement, $\delta(u)$, as:

$$\delta(u) = u - C_{comp}F_{comp}(u) \qquad (14)$$

where C_{comp} is the elastic compliance of the composite. The bridging stress, $\sigma_{br}(\delta)$ is then expressed by:

$$\sigma_{br}(\delta) = \frac{V_f}{l}\left\{\begin{array}{l} \dfrac{1-V_f}{V_f}E_m\delta\, e^{-\left(\frac{\delta}{b_m}\right)^{a_m}} + E_f u\, e^{-\left(\frac{\delta}{b_f}\right)^{a_f}} + \\[2ex] + \dfrac{2klL_p\tau}{R_f}\left[e^{-\frac{\delta-\delta^*}{L_p}} - e^{-\frac{u-\delta^*}{L_p}\left(\frac{\delta-\delta^*}{b_f}\right)^{a_f}} \right] \end{array}\right\} \qquad (15)$$

Where δ^* is the crack opening displacement calculated by Eq. 14 for $u = u^*$.

EXPERIMENTAL

The proposed model is validated against experimental values of bridging stresses captured directly at the microscale on individual bridging fibres, during real testing time of a continuous SiC-Nicalon fiber reinforced glass-ceramic matrix cross-ply laminate.

The matrix consisted of magnesium, aluminium, silicon and lithium oxides (MgO, Al$_2$O$_3$, SiO$_2$ and LiO$_2$) and was processed via the sol-gel route. Double-edge notch (DEN) specimens of dimensions $120 \times 12 \times 2$ mm^3 (l $\times$ w $\times$ t) and $120 \times 10 \times 3$ mm^3 (l $\times$ w $\times$ t) were machined from 2mm and 3mm thick plates of [0/90]$_{2s}$ fibre orientations. It entails that, for the specific laminates, k=0.5. The notch-to-width ratio was maintained at 0.4.

Testing was interrupted periodically and the stress on individual bridging fibres visible within the separating crack franks after matrix cracking was measured by a scanning Raman microprobe. The spectroscopic setup used for the collection of bridging stresses using the LRM technique has been presented elsewhere (Dassios et al, 2003a).

Table 1. Material and specimen constants

Parameter	Symbol	Value
Gauge length	l	25 mm
Cross sectional area	S	14.4 mm^2 (plate t=2mm) 18 mm^2 (plate t=3mm)
Fibre radius	R_f	7 μm 7 (Simon and Bunsell, 1984)
Fibre volume fraction	V_f	0.35 (Drissi-Habti, 1997)
Mean pull-out length	L_p	690 mm (Brenet et al, 1996)

Table 2. Initial conditions for the regression

Parameter	Initial Values	Regression outputs		Bibliographic Value
Fibre		*DEN1*	*DEN2*	
SiC-Nicalon Young's modulus, E_f, GPa	250	190	214	200 (Drissi-Habti, 1997)

Fibre shape parameter, α_f	6	2.525	2.520	2.3-2.7 (Simon and Bunsell, 1984)
Fibre location parameter, b_f, mm	0.15	0.105	0.090	N/A
First fibre failure displacement, u^*, mm	0.05	0.020	0.021	N/A
Matrix				
Matrix Young's modulus, E_m, GPa	80	63	71	70 (Brenet et al, 1996)
Matrix shape parameter, α_m	10	1.895	1.889	N/A
Matrix location parameter, b_m, mm	0.05	0.035	0.039	N/A
Interface				
Interfacial shear strength, τ, MPa	5	3.04	3.21	2-5 (Brenet et al, 1996)

RESULTS AND DISCUSSION

Efficiency of the model

The load-displacement version of the model, Eq. 13, was used to assess the experimentally recorded behaviour of the composite. The regression was performed iteratively under the x^2 reduction criterion. Specimen and material properties such as the gauge length, l, cross-sectional area, S, fibre radius, R_f, fibre volume fraction, V_f, and mean pull-out length L_p were held constant; the values used in the model for these properties are presented in Table 1. The remaining parameters in Eq. 13 were left to unconditionally vary during the regression, however initial values were provided and are presented in Table 2. The initial values for the elastic moduli and interfacial shear strength in Table 2 are approximate engineering values, the shape parameters for the matrix and fibres are approximate Weibull moduli values for monolithic ceramics and fibres respectively, while the location of first fibre failure, u^* is calculated at the conventional 0.2% strain limit. The location parameters for the matrix and fibres distributions are empirically set to u^* and $3u^*$, respectively.

A number of restraining conditions were imposed to the regression procedures in order to realistically relate the succession and interaction of individual contributions. First, to simulate the CMC fracture characteristic of matrix cracking completion before the maximum load is attained, the corrsponding contribution, Eq. 4, was constrained in displacements lower than those of the maximum load. Second, the surviving fibre contribution was not allowed to extend into the interfacial pull-out regime. Third, the displacement of first fibre failure, u^*, used to denote the appearance of the interfacial term, was set to coincide with the displacement on first fibre failure (onset of deviation of the intact fibre dictribution from linearity).

The experimental load-displacement curves of DEN specimens with different thicknesses and widths were used for testing the efficiency of the model. Two typical cases are presented herein. We named DEN 1 a specimen with a width of 12mm and a thickness of 2mm, and DEN 2 a 10mm-wide and 3mm-thick specimen. The output parameters of the regression (best-fit values) are listed in Table 2 along with reference values for the same properties found in the bibliography. The computed behaviours are plotted alongside the experimental results in Fig. 2. In order to improve readability of the figure, displayed experimental data (hollow circle symbols) are reduced to 1/50 of the captured points.

Fig. 2. Experimental (hollow cycles data) and

theoretically modelled (straight lines) load-displacement curves for 2 DEN specimens of different sizes. Also shown are the deconvolutions of the models into the matrix (dashed lines), fibres (dotted lines) and interface (dash-dotted lines) contributions.
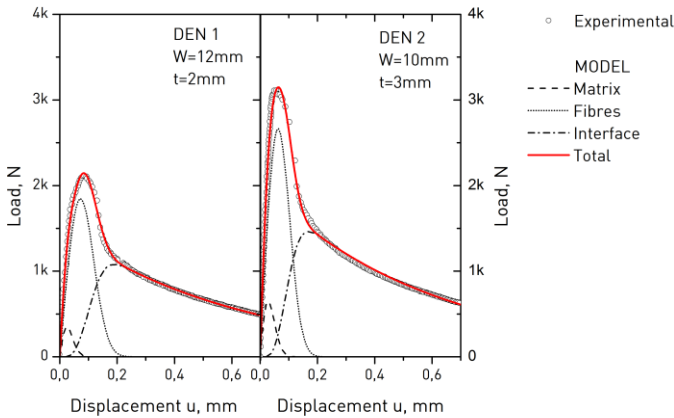
The model was very efficient in assessing the experimental load-displacement response of the composite with all coefficients of correlation remaining higher than 99.5%. By observation of the regression output values (Table 2), three important conclusions can be drawn: First, the output values of both regressions varied by no more than 10% among the two specimens with different dimensions. Hence the modelled behaviour can be considered a material-intrinsic fracture descriptor for the specific composite system. Second, the computed shape parameter for the fibres (directly equivalent to their Weibull modulus) exhibits minimal scatter and compares favourably with the previously established value for fibres in air. This finding indicates that fibres in the composite fail under a pattern similar to that in air, hence their failure mechanism is not critically affected by the interaction with the moderate interface. Thirdly, the statistical interfacial shear stress computed by the regression, with high accuracy, at around 3MPa, is a finding of particular importance given the large scatter of bibliographically available values and the complexity associated with the experimental measurement of this property.

A mean composite modulus value of 115GPa was computed via the rule of mixtures using the modelled constituents' moduli, which compares favourably with the bibliographically available value of 123GPa for the specific composite system (Drissi-Habti, 1997). This finding is a separate measure of the efficiency of the model.

Experimental vs macromechanical bridging stresses
The modelled bridging stress distribution and the individual fibres and interface contributions are computed through Eq. (14) and (15) and plotted in Fig. 3.

Fig. 3. Macromechanical (hollow cycles data) and theoretically modelled (straight lines) bridging stress distributions for the specimens of Fig. 1. The crack opening displacement corresponds to the non-linear displacement of the system.
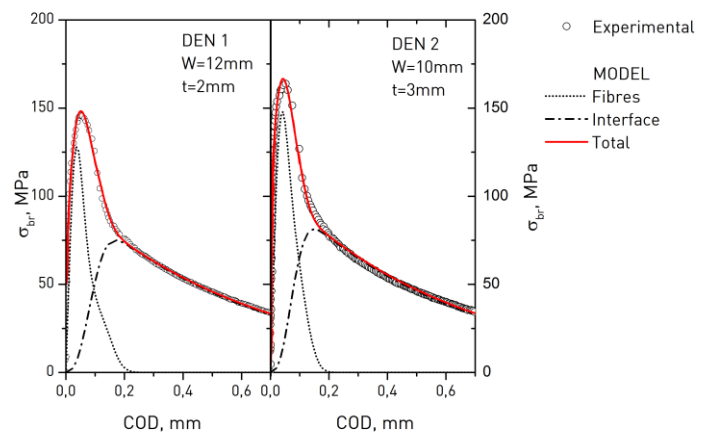
Typical bridging strain distributions, captured in situ and directly at the microscale via the LRM technique, are plotted as a function of normalized position along the un-notched ligaments of the specimens in Fig. 4. In each specimen, at least three steps of LRM scanning of the ligaments were performed at key instances of the loading procedure: the first step within the pure bridging regime was chosen in order to capture the axial stress component on surviving fibres independently. The following step rested within

the mixed regime of fibre and interfacial interaction, where a part -but not all- of the fibres had failed and were undergoing pull-out, while a third step was within the pure interfacial regime where only frictional forces give rise to an axial stress component. The instant loading level for the composite is shown in the smaller plots to the left of each distribution. The left-side y-axes of Fig. 4 represent the experimentally measured wavenumber shift, while the right y-axis give the LRM-equivalent strain corresponding to the specific shift. Shown in hollow cycle symbols are the mean values of 3-5 LRM strain measurements on the same fibre. The associated standard deviation of each set of measurements is shown as error bar.

Fig. 4. Directly measured bridging strain distribution profiles at the microscale.
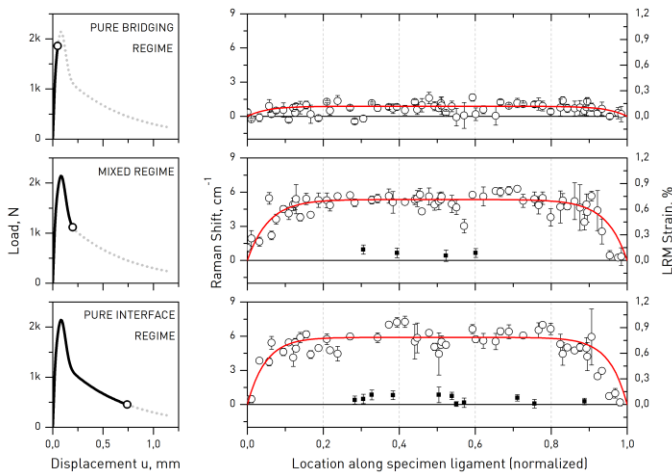
Strain build-up, from zero to a plateau value, was observed within a 10% distance from each notch root, independently of load level. The plateau value remained uniform throughout the rest of the ligament. This finding indicates a possible relaxation in fibre strain around the notch roots due to local stress concentration. The experimental data were fitted with exponential functions of the form:

$$f(x) = \begin{cases} c_1 e^{-b_1 x} & 0 \le x < 0.5 \\ c_2 e^{b_2(x-1)} & 0.5 \le x < 1 \end{cases} \qquad (16)$$

where x is the normalized location along the ligament, and c_i and b_i are constants. The regressions are shown as solid lines in Fig. 4.

Square symbols data in Fig. 4 correspond to load-free fibers that have failed either within the crack opening or have prematurely pulled-out completely. As expected, the number of such data increases with loading. The experimental bridging stress can be calculated by multiplying the plateau values of the bridging strain distributions by the modelled value fiber's Young's modulus, *ca* 200 GPa. The experimental bridging stresses that were measured directly via LRM on 3 DEN specimens are plotted in comparison to the macromechanical counterpart in Fig. 5. The observed inverse relation between the two stresses is characteristic of the different length scale over which the two stresses are expanding. The Raman stress of individual fibres that deform linear-elastically up to failure is local, at the microscale, and monotonically increasing up to failure. On the other hand, the macromechanical value is affected by the decreasing number of intact fibers due to successive failure while assuming a constant cross sectional area. The observed discrepancy is a magnification of the typical strength/failure stress controversy in simple tension tests where specimen "necking" leads to nominal failure stress values lower than the maximum.

Fig. 5. Macromechanical and experimental bridging stresses.
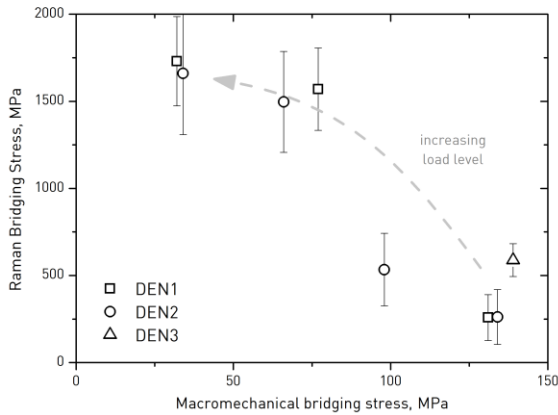
Reverse usage of the model

The efficiency of the established model in *predicting* the fracture behaviour of a composite material with similar energy dissipation characteristics, appears to be of particular interest. In fact, if all experimentally measurable parameters appearing in Table 2 are known for the specific material system the model can indeed provide the mechanical behaviour of the composite and a test is not needed.

To demonstrate this potential of our model, we will use it to inversely predict the mechanical response of 3 hypothetical composite systems with different energy dissipation potentials. The first case study is a composite with an almost negligible bridging mechanism where fibres fail abruptly within the matrix environment soon after matrix cracking. We will model this system with a large fibre shape parameter allowing for a narrow failure distribution.

Table 3. Model parameters for different case studies

The second case concerns a composite of minimal interfacial energy dissipation characteristics, associated with small pull-out lengths. The third material is one with strong interfacial bonding, modelled by a high value of τ. Table 3 lists the values of all properties entering the model for each case study. The values of all unvaried properties where kept equal to the mean values obtained previously for the specific CMC. A 12mm wide, 2mm thick specimen with 0.4 notch-to-width ratio is assumed. The corresponding predicted load-dislacement curves are shown in Fig. 6.

Fig. 6. Predicted load-displacement curves for composite systems with different energy dissipation mechanisms
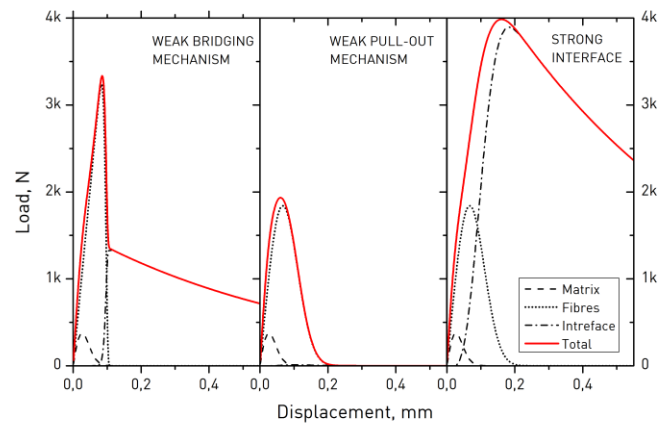
Parameter	Case 1 Weak Bridging	Case 2 Weak pull-out	Case 3 Strong interface
Specimen			
Gauge length, l, mm	25	25	25
Cross sectional area, S, mm^2	14.4	14.4	14.4
Fibre radius, R_f, μm	7	7	7
Fibre volume fraction, V_f	0.35	0.35	0.35

Fibre			
SiC-Nicalon Young's modulus, E_f, GPa	202	202	202
Fibre shape parameter, a_f	**20**	2.522	2.522
Fibre location parameter, b_f, mm	0.097	0.097	0.097
First fibre failure displacement, u^*, mm	0.020	0.020	0.020
Matrix			
Matrix Young's modulus, E_m, GPa	67	67	67
Matrix shape parameter, a_m	1.892	1.892	1.892
Matrix location parameter, b_m, mm	0.037	0.037	0.037
Interface			
Interfacial shear strength, τ, MPa	3.12	3.12	**10**
Pull-out length, μm	700	**50**	700

The effect of the bridging mechanism in the overall fracture behavior of a brittle matrix composite is demonstrated in the first graph of Fig. 6. The absence of the particular mechanism leads in a sharp decrease in intact fibre contribution and in an almost linear-elastic mechanical behavior up to fracture. Hence the energy dissipation potential of the bridging mechanism is critical in controlling the composite failure mode. However, since the pull-out mechanism has not been neglected, the specimen separates with progressive fibre ends disengaging from the matrix environment, giving rise to exponentially decreasing frictional forces. By comparison with the first graph of Fig. 2, it is observed that the narrow failure distribution is associated with a 50% increase in the maximum load attainable by the laminate. The form of the modeled curve is identical to that predicted by other fundamental studies (Thouless and Evans, 1988).

The effect of pull-out on the macromechanical response the composite is shown in the center graph of Fig. 6. The linear elastic part of the curve and the maximum load are identical to the general case (left graph in Fig. 2), however the frictional "tail" of the curve is not present and composite load appears to decrease smoothly, as bridging fibres progressively fail within the crack flanks. The dramatic effect of the interface on the mechanical performance of the composite is demonstrated in the third (right) graph of Fig. 6. A three-fold increase in the value of the

interfacial shear strength (ISS), τ, leads not only to a 100% increase in the maximum load by mainly to a radical increase in the energy dissipation potential of the material after that point. According to the aforementioned model formulation rationale, higher ISS values are related to increased frictional forces during sliding of the fibres' surfaces along the debonded interface, a phenomenon that gives rise to higher shear loads with accordingly high axial components.

Based on the above observations, it is entailed that the precision in measuring the values of the composite constituents' properties, and mainly of the interface, defines the expected ability of the model to predict the macromechanical behavior of the material. However the model can reconcile any material property ignorance. One tensile test is sufficient for the model to establish these values, so that it can subsequently be used to intrinsically describe the composite's mechanical performance.

Comparison with a fundamental model
Based on weakest link statistics and earlier studies, Thouless and Evans (1988) have offered a highly-referenced fundamental model for assessing the fracture behavior of ceramic matrix composites. The derivation of their model was based exclusively on the mathematical formulation of the physics and statistics of the fracture mechanisms of CMCs, which contrasts the phenomenological character of the model

proposed in the current study. According to their model, the equation that relates the composite stress after first matrix crack, σ, to the instant crack opening displacement, δ, is given by:

$$\frac{\sigma(\delta)}{V_f} = \left(\frac{\delta}{v}\right)^{\frac{1}{2}} e^{-a} + \frac{1-e^{-a}}{(1+\xi)(1+m)}\left[\gamma - \frac{\Sigma(m+1)}{2E_f}\frac{\delta}{v}\right] \quad (17)$$

where Σ is the value of stress for which 50% of the fibres have failed, m is the Weibull shape parameter of the fibres and α, v, ξ and γ are given by:

$$a = \left(\frac{\delta}{v}\right)^{\frac{m+1}{2}} \quad (18)$$

$$v = \frac{\Sigma^2 R_f}{2\tau E_f(1+\xi)} \quad (19)$$

$$\xi = \frac{E_f V_f}{E_m(1-V_f)} \quad (20)$$

$$\gamma\left(\frac{m+2}{m+1}, a\right) = \int_0^a \beta^{\frac{1}{m+1}} e^{-\beta} \mathrm{d}\beta \quad (21)$$

The first term of the right-scale of equation 17 represents the bridging stress while the second term is the pull-out contribution. Using the mean values obtained previously for the CMC of our study (Table 2), the Thouless-Evans approach to the mechanical behavior of our material is calculated through equations 17-21. The result is plotted along the experimental behavior and the model of the current study in Fig. 7.

By examination of Fig. 7 it is observed that the reference model cannot fully assess the fracture behavior of the current CMC. While the maximum bridging stress is close to the experimentally recorded value, the decrease is stress after that instance is much steeper in the T-E model than it is in reality. Secondly, the experimental transition from the fibre regime to the interfacial regime is gradual, in contrast to the T-E expectations. Thirly, the interfacial contribution appears to decrease linearly in the reference model while both experiment and the

currently proposed model agree to an exponential decrease.

Figure 7. Comparison of experimental data to modeled behaviours
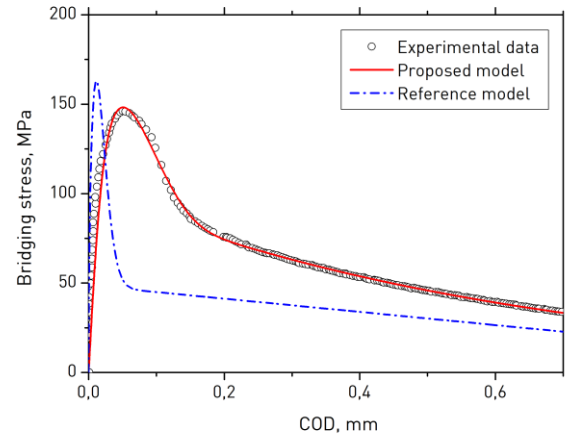
CONCLUSIONS

The energy dissipation mechanisms of CMCs were explained, macromechanically analyzed, mathematically simulated and directly measured at the microscale on a SiC-fibre reinforced glass-matrix composite using the LRM method. The performance of the phenomenological load-displacement expression, which was established by coupling the individual contributions of the matrix, fibres and the interface, was successfully evaluated across the experimental load-displacement response of the material. All regression output parameters ranged within 10% among double-edge notch samples of different dimensions. The established expression was thereafter used inversely to predict the mechanical response of various hypothetical composite systems with different fibre and interfacial energy dissipation potentials, as well as to understand their magnitude and interactions. Interfacial shear strength was identified as the key parameter dominating the mechanical behaviour of CMCs. The real stress values measured on individual fibres using LRM, were significantly higher than both their macromechanical

and theoretical counterparts, due to the real-versus-nominal stress discrepancy found in tensile configurations.

REFERENCES

Brenet, P., F. Conchin, et al. (1996). "Direct measurement of crack-bridging tractions: A new approach to the fracture behaviour of ceramic/ceramic composites." Composites Science and Technology 56(7): 817-823. Cox, B.N., *Acta Mater.*, 1991, **39**, 1189.

Dassios, K. G., C. Galiotis, et al. (2003). "Direct in situ measurements of bridging stresses in CFCCs." Acta Materialia 51(18): 5359-5373.

Dassios, K. G., V. Kostopoulos, et al. (2007). "A micromechanical bridging law model for CFCCs." Acta Materialia 55(1): 83-92.

Dassios KG, (2003), PhD Thesis, Dept. of Mech Eng and Aeronautics, University of Patras, Greece

Drissi-Habti, M. (1997). "Assessment of the Mechanical Behaviour of SiC Fibre Reinforced Magnesium Lithium Aluminosilicate Glass-Ceramic Matrix Composite Tested under Uniaxial Tensile Loading." Journal of the European Ceramic Society 17:37-39

Fett, T. and D. Munz (1995). "Bridging Stress Relations for Ceramic Materials." Journal of the European Ceramic Society 15(5): 377-383.

Fett, T., Munz, D., Geraghty, R.D., White, K.W. (2000). "Influence of specimen geometry and relative crack size on the R-curve". Eng. Fract. Mech. 66: 375-386

Foote, R.M.L., Mai, Y.-W. and Cotterell, B. (1986). "Crack growth resistance curves in strain-softening materials". J. Mech. Phys. Solids, 34: 593-607

Hu, X.Z., Mai, Y.W. (1992). "A general method for determination of crack-interface bridging stresses". J. Mater. Sci. 27:3502-3510

Jacobsen TK, Sorensen BF. (2001). "Mode I intra-laminar crack growth in composites — modelling of R-curves from measured bridging laws" Compos. Part A-Appl. S. 32:1-11.

Llorca, J. and Singh, .N. (1991). "Influence of Fiber and Interfacial Properties on Fracture Behavior of Fiber-Reinforced Ceramic Composites" J. Am. Ceram. Soc., 74, 2882-2890

NASA Columbia Accident Investigation Board Final Report, August 26, 2003, http://spaceflight.nasa.gov/shuttle/archives/sts-107/investigation/CAIB_medres_full.pdf

Pappas, Y. Z. and V. Kostopoulos (2001). "Toughness characterization and acoustic emission monitoring of a 2-D carbon/carbon composite." Engineering Fracture Mechanics 68(14): 1557-1573.

Rausch, G., M. Kuntz, et al. (2000). "Determination of the in situ fiber strength in ceramic-matrix composites from crack-resistance evaluation using single-edge notched-beam tests." Journal of the American Ceramic Society 83(11): 2762-2768.

Simon, G. and Bunsell, A.R. (1984). "Mechanical and structural characterization of the Nicalon silicon carbide fibre", J. Mater. Sci., 19, 3649-3657

Sorensen, B. F. and T. K. Jacobsen (1998). "Large-scale bridging in composites: R-curves and bridging laws." Composites Part a-Applied Science and Manufacturing 29(11): 1443-1451.

Sutcu M. (1989). "Weibull statistics applied to fiber failure in ceramic composites and work of fracture" Acta Mater. 37:651-661

Thouless, M. D. and A. G. Evans (1988). "Effects of Pull-out on the Mechanical-Properties of Ceramic-Matrix Composites." Acta Metallurgica 36(3): 517-522.